

Lawrence Berkeley National Laboratory

LBL Publications

Title

Revealing the working mechanism of a multi-functional block copolymer binder for lithium-sulfur batteries

Permalink

<https://escholarship.org/uc/item/69x0c54z>

Authors

He, Xin
Liu, Zhimeng
Gao, Guoping
et al.

Publication Date

2021-08-01

DOI

10.1016/j.jechem.2020.10.002

Peer reviewed

Revealing the working mechanism of a multi-functional block copolymer binder for lithium-sulfur batteries

Xin He^{a#}, Zhimeng Liu^{a#}, Guoping Gao^{b#}, Xiaotao Liu^c, Michal Swietoslowski^a, Jun Feng^d, Gao Liu^a, Lin-Wang Wang^b, Robert Kostecki^{a*}

^a Energy Storage & Distributed Resources Division, Lawrence Berkeley National Laboratory, 1 Cyclotron Road, Berkeley, CA, 94720, USA

^b Materials Sciences Division, Lawrence Berkeley National Laboratory, Berkeley, CA, 94720, USA

^c The Molecular Foundry, Lawrence Berkeley National Laboratory, Berkeley, CA, 94720, USA

^d Department of Materials Science & Engineering, Southern University of Science and Technology (SUSTech), Shenzhen 518055, Guangdong, China

These authors made equal contributions

* Corresponding author e-mail address: r_kostecki@lbl.gov

Keywords: Lithium sulfur batteries, Polymer binder, Block copolymer, Ultraviolet-visible spectroscopy, X-ray absorption spectroscopy

Abstract

The lithium-sulfur (Li-S) battery is one of the most promising substitutes for current energy storage systems because of its low cost, high theoretical capacity, and high energy density. However, the high solubility of intermediate products (i.e., lithium polysulfides) and the resultant shuttle effect lead to rapidly fading capacity and a low coulombic efficiency, which hinder the practical application of Li-S batteries. In this study, block copolymers are constructed with both an ethylene oxide unit and a styrene unit and then used as binders for Li-S batteries. Electrochemical performance improvements are attributed to the synergistic effects contributed by the different units of the block copolymer. The ethylene oxide unit traps polysulfide, which bonds strongly with the intermediate lithium polysulfide, and enhances the transport of lithium ions to reach high capacity. Meanwhile, the styrene unit maintains cathode integrity by improving the mechanical properties and elasticity of the constructed block copolymer to accommodate the large volume changes. By enabling multiple functions via different units in the polymer chain, high sulfur utilization is achieved, polysulfide diffusion is confined, and the shuttle effect is suppressed during the cycle life of Li-S batteries, as revealed by operando ultraviolet-visible spectroscopy and S K-edge X-ray absorption spectroscopy.

1. Introduction

Electrochemical energy storage systems with high energy density, low cost, and long cycle life have been sought for numerous applications, including modern mobile electronic devices, electric vehicles, and the sustainable energy industry [1-4]. Among the various energy storage candidates, lithium-sulfur (Li-S) batteries stand out because the abundance of sulfur, and it has low cost, high theoretical capacity (1675 mAh g^{-1}), and high theoretical energy density (2567 Wh kg^{-1}) [5-7]. Despite these advantages, numerous practical problems have prevented the large-scale use of Li-S batteries. These problems include the low electrical conductivity of sulfur [5], the dissolution and diffusion of the lithiated polysulfide (Li_2S_x , $2 \leq x \leq 8$) in electrolyte [6], deposition of non-soluble and insulating Li_2S on the electrode due to the shuttle effect of lithium polysulfide, and sulfur volume expansion/contraction during the discharge/charge process [7], which leads to dramatically lower discharge capacity and short cycle life.

In order to address these challenges, various carbon/sulfur matrices with [optimized](#) structures have been proposed, such as the integration of sulfur with porous carbon [8], graphene [9], graphene oxide [10-13], and carbon nanotubes [14-17]. Such unique structures can efficiently improve electronic conductivity and prevent the dissolution, diffusion, and shuttling of lithium polysulfides by physical encapsulation [18,19]. An alternative route is to use the chemical adsorption of the functional polymer binders in the sulfur cathode to immobilize polysulfides [20-22]. Various chemical bonding approaches have been employed to meet the required chemical,

electrochemical, and mechanical stability in the cell [23-26]. Polyvinylidene fluoride (PVdF) is a conventional non-reactive polymer binder in Li-S batteries that acts as an effective adhesion agent to connect the active materials and conductive additives together, and then steadily adhere them to the current collectors. However, PVdF can only provide physical adhesion, with limited ability to form coordination-like bonds with the intermediate lithiation products [19], resulting in serious polysulfide dissolution in the aprotic electrolyte during operation.

Recently, various types of polymer—with functional groups such as hydroxyl (-OH) [20], carboxyl (-COOH) [21], nitrile (-CN) [22], ethylene oxide (-CCO-) [15], and amino (-NH₂) [31,32] groups—have been introduced as binders to provide the strong affinity to absorb or trap polysulfide intermediates, resulting in improved cycling performance. In addition, copolymer binders combined with rich functional groups were designed to allow the binder to achieve multiple benefits. For example, the natural polymer gum arabic (a mixture of polysaccharides and glycoproteins) provides excellent mechanical properties to buffer the volume change of sulfur and form chemical bonds with the sulfur species to subsequently confine them within the electrode [21].

Inspired by the advantages of functional groups, in the present study, a synthesized block copolymer constructed with an ethylene oxide unit and a styrene unit is used as a binder for Li-S batteries. The ethylene oxide unit can effectively transfer lithium ions [25] and introduce a highly hydrophilic functional site for trapping the polysulfides [26]. However, ethylene oxide easily swells in electrolyte, making it difficult to maintain cathode integrity [18]. The styrene unit enhances the mechanical properties and elasticity of the constructed block copolymer to accommodate the large volume changes. Therefore, combining the ethylene and styrene units in a polymer chain can maintain electrode stability, further confine polysulfide diffusion, and suppress shuttle effects on cycle life. Operando X-ray adsorption spectroscopy (XAS), in situ UV-visible spectroscopy, and X-ray photoelectron

spectroscopy (XPS) confirm that the block copolymer is an effective binder for suppressing polysulfide dissolution in the electrolyte.

2. Experimental methods

2.1 Electrode preparation

Sulfur powder (Sigma-Aldrich) and Super C45 (TIMCAL) were first mixed by high energy ball milling for 24 hours, and the resulting composite was added into the binder solution to form an electrode slurry. The PVdF binder was dissolved in N-Methyl-2-pyrrolidone (NMP) solvent. The block copolymer binders, BC82 (with an 82% ethylene oxide unit in the polymer chain) and BC65 (with a 65% ethylene oxide unit in the polymer chain), were dissolved in tetrahydrofuran (THF) (Sigma-Aldrich). The composition of cathode slurry was sulfur: C45: binder = 60:30:10 (wt%). The slurry was mixed by ball milling for 6 hours to achieve a homogeneous distribution. Then, the slurry was coated onto an aluminum current collector with a doctor blade using an Elcometer motorized film applicator. The coated slurry was dried in a vacuum oven for 2 days at 50 °C and stored in an argon-filled glove box.

2.2 Cell assembly and testing

Coin cells (CR2032, MTI) were assembled in an argon-filled glove box with O₂ and H₂O content less than 0.1 ppm. Lithium metal foil was used as the anode, and polypropylene celgard 2400 was used as a separator. The electrolyte was 1M lithium bis(trifluoromethanesulfonyl)imide (LiTFSI) dissolved in a mixture of 1,3-dioxolane (DOL) and dimethoxyethane (DME) (1:1 by volume) with 1% LiNiO₃ as an additive to help passivate the surface of the lithium anode and reduce the shuttle effect. Into each cell were added 50 μL of electrolyte. The electrochemical performance was measured galvanostatically in a voltage window of 1.7–2.8 V on a Maccor series 4000 cell tester at 30 °C. The specific capacities were calculated based on the mass of sulfur in the electrodes.

2.3 Density functional theory (DFT) calculation

The DFT calculations were carried out using planewave DFT calculations implemented in the PWmat code[27,28] with norm-conserving SG15 pseudopotential. The exchange-correlation interactions were treated by the generalized gradient approximation in the form of the Perdew-Burke-Ernzerhof function [29,30]. The Van der Waals interaction was described by using the empirical correction in Grimme's scheme, i.e., DFT + D₂ [31]. The energy cutoff was set to 680 eV. The vacuum spaces in the b and c axes were 15 Å, enough to avoid the interaction between periodical images. The Brillouin zone was sampled by a Monkhorst-Pack 3×1×1 K-point grid. The adsorption energy (E_{ad}) of Li₂S_x ($x = 2, 4, 6, 8$) on the binder was calculated by Eq (1).

$$E_{ad} = E_{total} - E_{binder} - E_{Li_2S_x} \quad (1)$$

In which E_{total} , E_{binder} , and $E_{Li_2S_x}$ refer to the total energy of the binder with Li₂S_x absorbed, the energy of the binders, and the energy of Li₂S_x, respectively.

2.4 Ultraviolet-visible (UV-vis) spectroscopy

The concentration of lithium polysulfide (with an overall stoichiometric ratio matching Li₂S₆) solution applied in the in-situ UV-vis test was 0.5 mmol/L in DOL/DME (1:1 vol/vol). Within a UV quartz container, 0.1 g of binder were soaked in lithium polysulfide solution. The spectra were collected through the Cary 5000 UV-Vis-NIR every hour during the 24-hour recording period.

2.5 Operando X-ray absorption spectra

The operando sulfur K-edge XAS spectra were measured at beamline 5.3.1 at the Advanced Light Source, Lawrence Berkeley National Laboratory. The X-ray beam size was ~100 μm × 100 μm. The XAS spectra were collected in total fluorescence yield (TFY) mode and calibrated using elemental sulfur spectra by setting the position of the white line to 2472.2 eV. All the XAS spectra were measured under constant helium flow at 5 mL/min in the sample chamber and acquired continuously during the lithiation/delithiation process at a 0.1-C rate (1 C = 1675 mA g⁻¹). The background of the XAS

spectra was subtracted and normalized to the absorption pre- and post-edges. The cells used to perform operando XAS experiments were adapted from the CR2032 coin cells: a 2-mm diameter hole was drilled in the sulfur (cathode) side of the can, and then the hole was sealed with a 10- μm thick aluminum Mylar film (Heliumetech) to avoid electrolyte leaking, prohibit beam damage, and allow X-ray beam penetration. In order to investigate species evolution in the electrolyte and on the lithium surface during the lithiation/delithiation process, a 3-mm diameter hole was also drilled in the sulfur cathode to make the X-ray beam probe directly into the cell.

2.6 Scanning electron microscope (SEM) images

The morphology of the electrode surface was characterized with a JEOL JSM-7500F field emission SEM with an accelerating voltage of 15 kV using the high vacuum mode at room temperature. All electrodes were examined in the same conditions, including pristine electrode and electrode after one cycle. The cycled electrodes were disassembled in a glove box and flushed with dimethyl carbonate to remove electrolyte residue.

3. Results and discussion

As illustrated in Fig. 1(a), the chemical structure shows that the block copolymer contains abundant ethylene oxide groups, which can improve ionic conductivity and trap lithium polysulfide with different lengths [26]. The DFT calculation results show that the ethylene oxide unit in the polymer chain exhibits much stronger binding strength compared with the binding of PVdF to the polysulfide (Li_2S_x , $2 \leq x \leq 8$). In the solvent, the bonding energies of the ethylene oxide unit to Li_2S_2 and Li_2S_8 are -0.84 and -0.99 eV, respectively. These negative adsorption energy values indicate that the polysulfides prefer to be adsorbed on the ethylene oxide unit in the polymer chain rather than being extricated in the solvent. The stability and integrity of the electrode are ensured by the styrene unit, benefiting from its mechanical strength against volume change [32,33]. This mechanical property improves as the styrene unit content increases. Therefore, the

combination of ethylene oxide and styrene units enhances the polysulfide binding capability and the mechanical strength of the binder simultaneously.

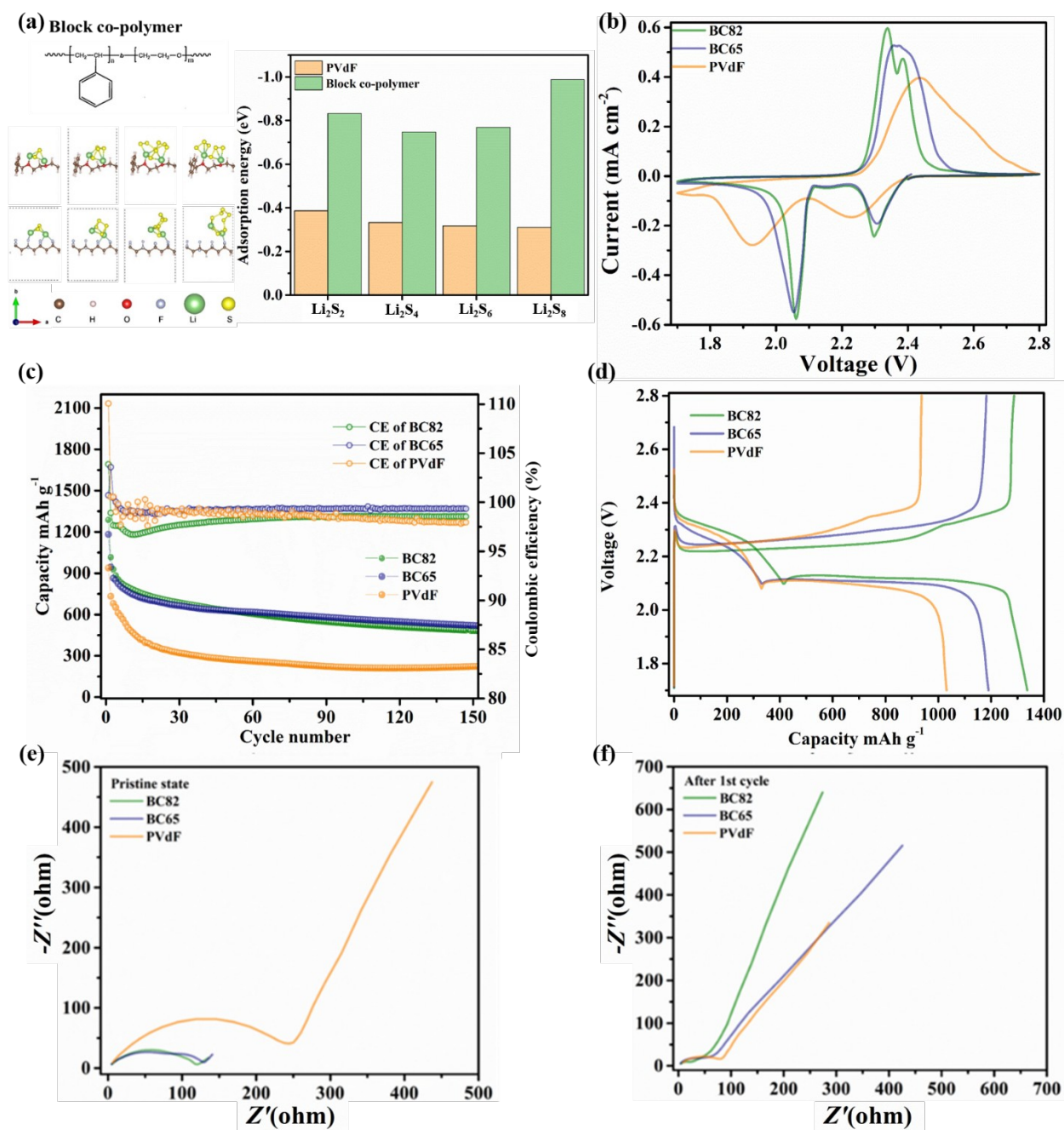


Fig. 1. (a) Chemical structure and adsorption energy of isolated Li_2S_x ($2 \leq x \leq 8$) to the PVdF and block copolymer in DOL/DME solvent; (b) CV curves of sulfur electrodes with different binders at a scan rate of 0.1 mV s^{-1} between 1.7 and 2.8 V; (c) cycling performance of sulfur electrodes with a sulfur loading of 0.8 mg cm^{-2} , 1st cycle at 0.1 C, and continued cycles at 0.2 C (CE: coulombic efficiency); (d) 1st charge and discharge curves of sulfur electrode

with different binders at 0.1 C; the electrochemical impedance spectra (EIS) of the cells assembled with different electrodes, which were obtained at pristine state (e) and after 1st cycle (f).

The electrochemical performance of the sulfur electrodes was first investigated via cyclic voltammetry (CV). Fig. 1(b) shows the CV curves of sulfur electrodes with different binder compositions. In the first cycle, all cathodes display a typical Li-S electrochemical behavior: one reduction peak appears at 2.15–2.45 V, representing the transformation from elemental sulfur (S_8) to high-order lithium polysulfide (Li_2S_x , $4 \leq x < 8$), and the second reduction peak appears at 1.7–2.15 V, attributed to the changing process from the high-order lithium polysulfide to low-order lithium sulfides (Li_2S_2/Li_2S). The oxidation peak around 2.2–2.8 V is attributed to the transition from lithium sulfides (Li_2S_2/Li_2S) to high-order polysulfide. Compared with the cathode using block copolymer as a binder, the cathode prepared with a PVdF binder displays the obvious potential shifts, indicating a serious polarization. Moreover, the peaks of cathodes with block copolymer are much narrower than the peak of a cathode with PVdF as a binder, verifying that block copolymer can significantly improve the reaction kinetics compared with PVdF. In addition, when the ethylene oxide content in block copolymer increases from 65% to 82%, the redox peaks become even sharper, indicating that the reaction kinetics can be further enhanced by increasing ethylene oxide content. Two oxidation peaks can be observed from the BC82 sample, demonstrating a significant improvement in reaction kinetics and roundtrip efficiency [34].

The improved reaction kinetics could also facilitate the activation of poorly conductive sulfur. As shown in Fig. 1(c), the electrode prepared with the BC82 binder delivers an initial discharge capacity of 1287 mAh g⁻¹ at 0.1 C (1 C = 1675 mA g⁻¹), which is 350 mAh g⁻¹ higher than the initial discharge capacity of the electrode with PVdF as a binder, indicating a higher proportion of sulfur is involved in the electrochemical process. After 50 cycles at 0.2 C, the electrode with PVdF as a binder retains a discharge

capacity of only 281 mAh g⁻¹, while the BC82 sample maintains a discharge capacity of 708 mAh g⁻¹. Although the initial discharge capacity of the BC65 sample is slightly lower than that of the BC82 sample, the BC65 sample better maintains the delivered discharge after long-term cycling. The much higher coulombic efficiency suggests a higher reversibility of active material from the electrochemical process, corresponding to the contribution of the styrene unit in the polymer chain. More styrene units could help to maintain the integrity of the electrode against large volume variation.

The first-cycle discharge and charge curves of electrodes with different binders are displayed in Fig. 1(d). The electrodes show similar two-plateau discharge curves; the first plateau at around 2.3 V is attributed to the formation of soluble long-chain polysulfide, and the second plateau at about 2.1 V is attributed to the formation of insoluble short-chain polysulfide, which is consistent with the CV curves in Fig. 1(b). The electrodes prepared with block copolymer show reduced voltage hysteresis, which can be explained by the much lower areal mass transfer resistance, as also proved by the electrochemical impedance spectra (EIS) of samples (shown in Fig. 1e and f) at pristine state and after the first cycle. With increased discharge capacity and voltage, the output energy of prepared Li-S batteries is significantly increased [35].

The morphology of sulfur cathodes prepared with different binders is shown in Fig. 2. From the SEM image of the fresh electrode with PVdF as a binder (Fig. 2a), the porous structure generated by the sulfur-carbon composite particles can be clearly observed. For the electrodes with block copolymer as a binder (Fig. 2c and e), obvious differences can be perceived before cycling. The binder “bridges” emerge between the sulfur-carbon composite, closely adhering and fully covering the particle to form an aggregated structure for the electrode due to the anchoring effect [36], indicating that the block copolymer binder has sufficient capability to connect the active components. With a higher proportion of ethylene oxide in the polymer chain, the electrode exhibits a smoother surface and more uniform structure.

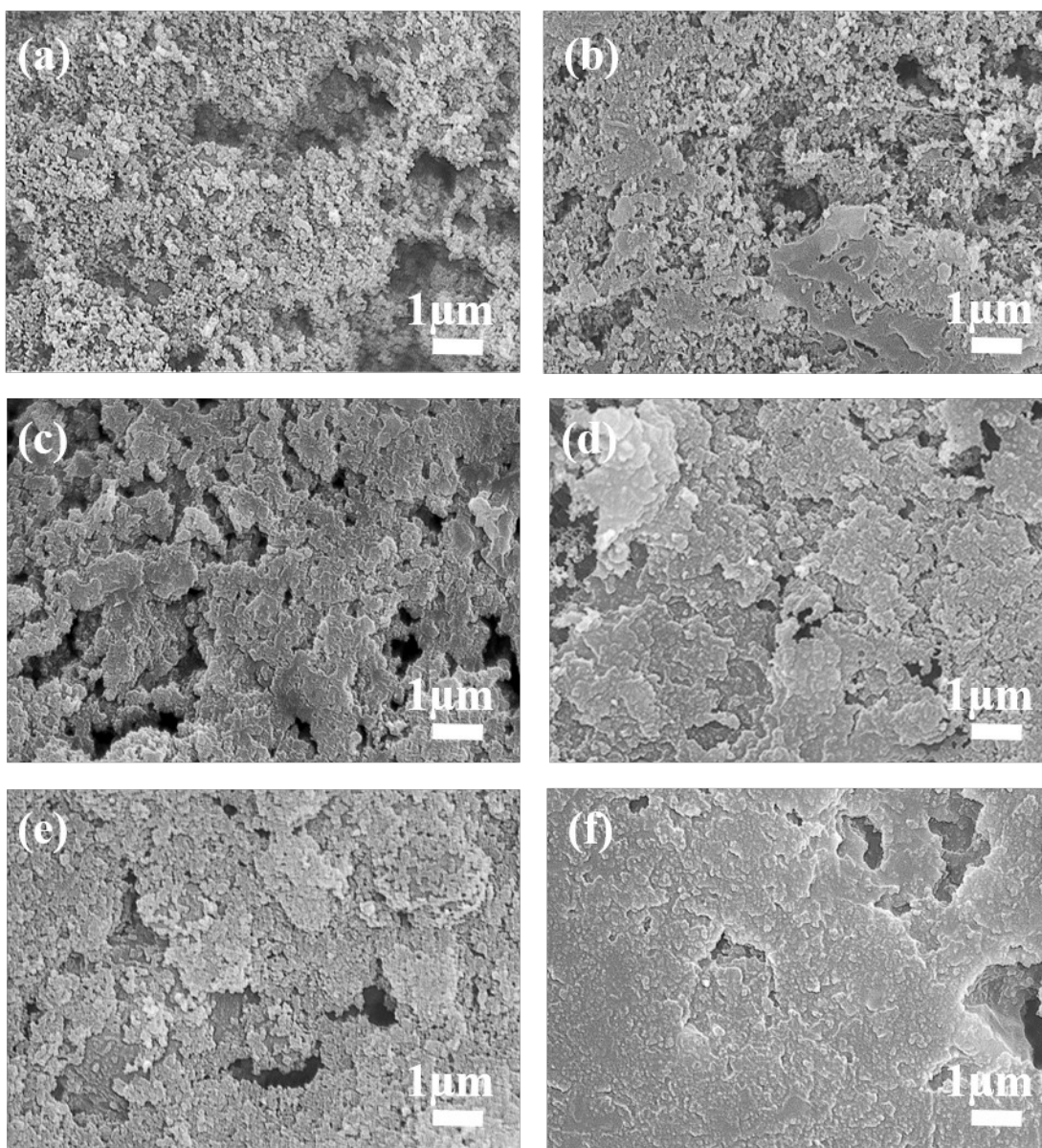


Fig. 2. SEM images of sulfur electrodes: (a), (c), and (e) are fresh sulfur electrodes with PVdF, BC65, and BC82 as binder, respectively; (b), (d), and (f) are sulfur electrodes cycled once at 0.2 C with PVdF, BC65, and BC82 as binder, respectively.

To study the influence of this multifunctional block copolymer binder on the morphological evolution of the electrode after an electrochemical process, the cells were disassembled after one cycle. The electrodes were thoroughly washed for morphology study. As shown in Fig. 2(b, d, and f), differences in morphology can be observed from cycled electrodes. The porous structure

remains in most areas of the electrode with PVdF as a binder, similar to the pristine state of electrode, which makes it difficult to limit the dissolution of polysulfide. The structures of the electrodes with block copolymer as a binder become denser, which may be due in part to the precipitation of solid sulfide species. The morphological change is more obvious for the BC82 sample, likely because the highly conductive ethylene oxide unit in the binder can facilitate the reaction kinetics but weakly controls particle swelling during the electrochemical process. Lithium polysulfide partly dissolves in the electrolyte owing to the weak mechanical property of the binder, and it is easier to precipitate solid-phase sulfur species because of the binder's strong trapping capability. Owing to the contribution from more styrene units in the polymer chain, the BC65 sample better maintains its original electrode structure, which means that a highly efficient synergistic effect can be achieved by using this binder.

Fig. 3(a) shows the color changes when different binders are soaked in the lithium polysulfide-containing electrolyte. A 0.5-mmol/L long-chain lithium polysulfide (with an overall stoichiometric ratio matching Li_2S_6) in DOL/DME solvent simulates the dissolution of lithium polysulfide in the electrolyte. The dark yellow color corresponds to a high content of lithium polysulfide in DOL/DME solvent. For the PVdF binder, the color of the electrolyte stays relatively dark even after 10 days, indicating that the lithium polysulfides are very stable in the solution. However, obvious color changes can be observed in the electrolytes with the block copolymers. They become markedly lighter over 3 days and fully clear in 10 days.

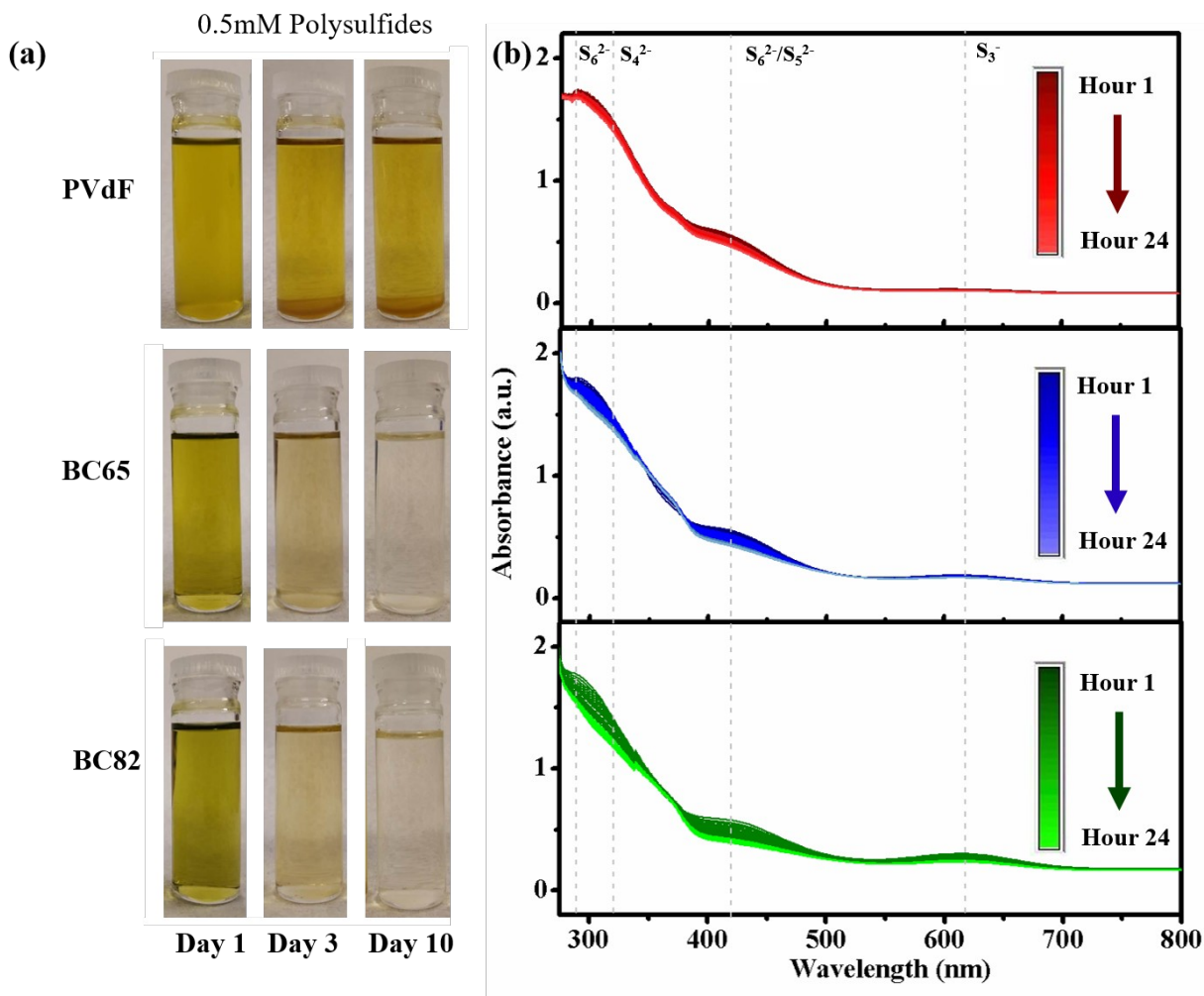


Fig. 3. (a) Photograph and (b) time-lapsed UV-vis absorbance spectra of the polysulfide solution after exposure to the different binders: PVdF (red), BC65 (blue), and BC82 (green).

To demonstrate the strong trapping capability of the block copolymer on lithium polysulfide (mainly Li_2S_6), in-situ adsorption measurement was conducted by adding 0.1 g of different binders to 5 mL of 0.5-mmol/L lithium polysulfide into DOL/DME solution to track the lithium polysulfide concentration evolution. Consistent with the pictures shown in Fig. 3(a), the UV-vis spectroscopy of the corresponding color changes for the contact of lithium polysulfide-containing electrolyte with different binders are essentially identical (Fig. 3b). The initial spectrum shows strong peaks at 287 and 426 nm, which can be attributed to the characteristic feature of Li_2S_6 [37,38]. The peak intensity represents the relative concentration of Li_2S_6 in

the solution. The concentration decreases significantly at these two wavelengths as the solution is exposed to block copolymer binders for 24 hours. The intensity of the Li_2S_6 feature continuously decreases over the whole test period, more obviously decreasing with a higher proportion of ethylene-oxide-containing binder, indicating that the ethylene oxide group can enhance the trapping capability of Li_2S_6 substantially. The UV absorption of electrolyte with BC82 also shows an obvious continuous decrease at 322 and 617 nm, which can be attributed to S_4^{2-} and S_3^- species [39,40]. This suggests that the ethylene oxide can trap various types of lithium polysulfide, and this advantage is more evident as the proportion of this unit is increased in the polymer chain. In contrast, when electrolyte is exposed to PVdF binder, the in-situ UV-vis spectra show an almost constant absorbance over 24 hours due to the weak physical adsorption of PVdF to polysulfide. These results clearly prove that the ethylene oxide group contained in block copolymer binder can strongly trap polysulfide in electrolyte through chemical bonding. The strong adsorption capability of ethylene oxide can explain the superior cycling performance of the block copolymer-based sulfur cathode as well: the intermediate polysulfide formed during the discharge/charge process can be trapped by the ethylene oxide group from the block copolymer binder in the sulfur cathode, which effectively suppresses the shuttle effect.

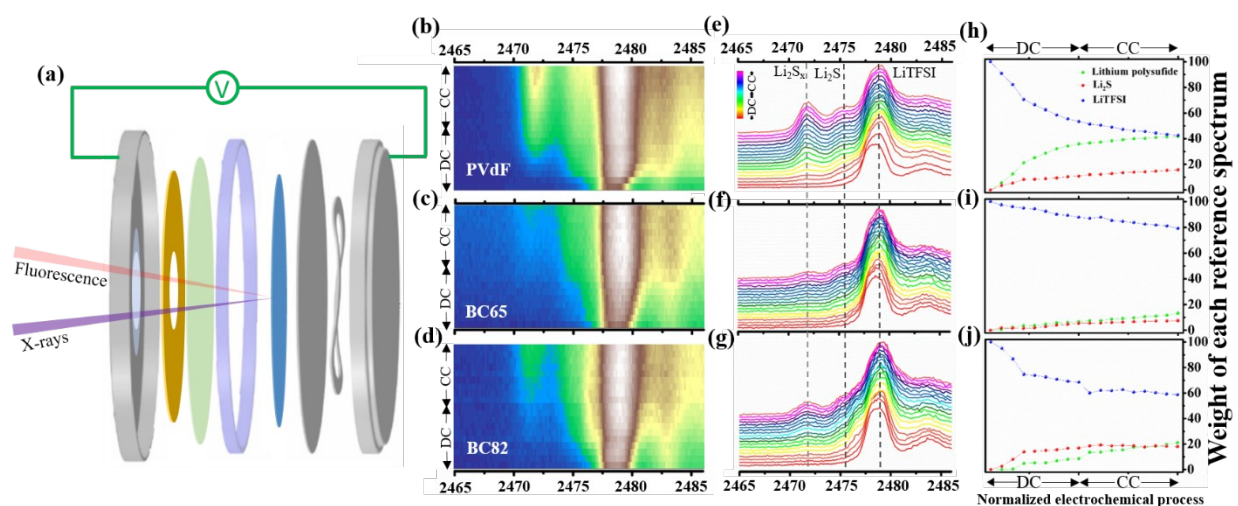


Fig. 4. (a) Schematic illustration of the coin cell design for operando XAS study. A $\varnothing 2$ -mm hole was drilled in the sulfur (cathode) side of the can; the hole was then sealed with a 10- μm thick aluminum Mylar film to avoid leaking and allow X-ray beam penetration. A $\varnothing 3$ -mm hole was also drilled in the sulfur cathode to make the X-ray beam probe directly into the electrolyte. From left to right: aluminum Mylar film, cathode cap, PVdF- or block copolymer-based sulfur cathode, gasket, separator, lithium anode, spacer, spring, and anode cap. Shown next are operando sulfur K-edge XAS mapping (b) with PVdF binder, representative XAS spectra (e), and the concentration of polysulfides, Li_2S , and LiTFSI (h) as a function of specific capacity based on the normalized peak area of (e) in electrolyte. Shown next are operando sulfur K-edge XAS mapping (c), representative XAS spectra (f) with BC65 binder, and the concentration of polysulfides, Li_2S , and LiTFSI (i) as a function of specific capacity based on the normalized peak area of (f) in electrolyte. Finally, shown are operando sulfur K-edge XAS mapping (d) with BC82 binder, representative XAS spectra (g), and the concentration of polysulfides, Li_2S , and LiTFSI (j) as a function of electrochemical process period based on the normalized peak area of (g) in electrolyte. (CC: charge; DC: discharge)

In order to reveal the working mechanism of block copolymer binder that is responsible for the enhanced electrochemical performance of Li-S batteries, operando S K-edge measurements were performed for the electrolyte area (without electrode) through the initial discharge-charge process. The result spectrum could also include the sulfur species on the surface of lithium because of the detection depth. The cell setup and design of the operando measurement are illustrated in Fig. 4(a). XAS is element-resolved and sensitive to the chemical bonding environment, which enables the investigation of sulfur speciation in the electrolyte due to the shuttle effect. A series of coin cells with an aluminum Mylar film sealed window on the sulfur electrode side were designed for X-ray penetration. The cells were galvanostatically cycled in the voltage range from 2.7 V to 1.7 V at a C-rate equivalent to 0.2 C. Fig. 4(b-d) show the operando S K-edge XAS maps, which are plotted for the XAS spectra intensity as a function of photon energy and electrochemical process time. The corresponding representative XAS spectra of cycled cells with different binders are shown in Fig. 4(e-g). Three main distinct features can be clearly observed from the XAS maps and their

corresponding spectra: the original highest peak at 2478.8 eV, which can be assigned to the sulfonyl groups in LiTFSI, and the fingerprint feature of polysulfide-Li₂S_x (2471.8 eV) and Li₂S (2475.4 eV) peaks as the result of the electrochemical process [41,42]. The intensity of the LiTFSI peak decreases gradually with the proceeding of the discharge process owing to the continued increase of lithium polysulfide concentration in the electrode from the lithiation of the sulfur electrode, which leads to the peak position shift to higher energies as a function of discharge time as well.[43] Two neighboring peaks near the position of LiTFSI at 2478.0 and 2482.0 eV are attributed to SO₃²⁻ and SO₄²⁻ groups, respectively [44]. The appearance of these two peaks probably relates to the formation of solid-state electrolyte interphase on the surface of the lithium anode [45]. The biggest differences in the XAS map are mainly located at the positions of Li₂S_x and Li₂S. The appearance of these peaks occurs at the early stage of the discharge process for the cell with PVdF as a binder, indicating the dissolution of polysulfide in electrolyte. The dissolved polysulfide can easily migrate between the electrodes, resulting in a serious polysulfide shuttle effect. However, these peaks appear much later and reach much lower intensity for the block copolymer, which proves the strong trapping capability of polysulfide by the block copolymer binder. As shown in the XAS map and selected spectra, the BC65 base cell shows more obvious advantages than the BC82 sample, because the presence of polysulfide only occurs at the final stage of the charge process. This result suggests that high mechanical strength is also a critical property for the design of a binder during cell preparation. Overall, a binder combining well-balanced trapping capability and mechanical strength could better suppress the dissolution of polysulfide.

In order to quantify the concentrations of LiTFSI, Li₂S_x, and Li₂S in the electrolyte during the initial discharge-charge process, the relative evolution of corresponding peak area is plotted as a function of electrochemical process period, shown in Fig. 4(h-j). The significant changes mainly occur during the discharge process, with a decrease in the concentration of LiTFSI

and increase in Li_2S_x and Li_2S , which agrees with the lithiation of sulfur to Li_2S_x and subsequent dissolution of partial Li_2S_x into the electrolyte. More clearly, even though BC82 could more sufficient trap polysulfide, the content of polysulfide in the electrolyte still reaches a much higher level than BC65, which emphasizes the point that a binder should be able to confine Li_2S_x effectively while maintaining electrode integrity. During the charging process, the concentrations of each component show little changes, suggesting that the dissolved polysulfide can only remain in the electrolyte. This phenomenon reveals that some of the polysulfide cannot be further involved in the electrochemical process, and the irreversibility could directly explain the high coulombic efficiency of the first cycle and obviously fading capacity during the following cycles.

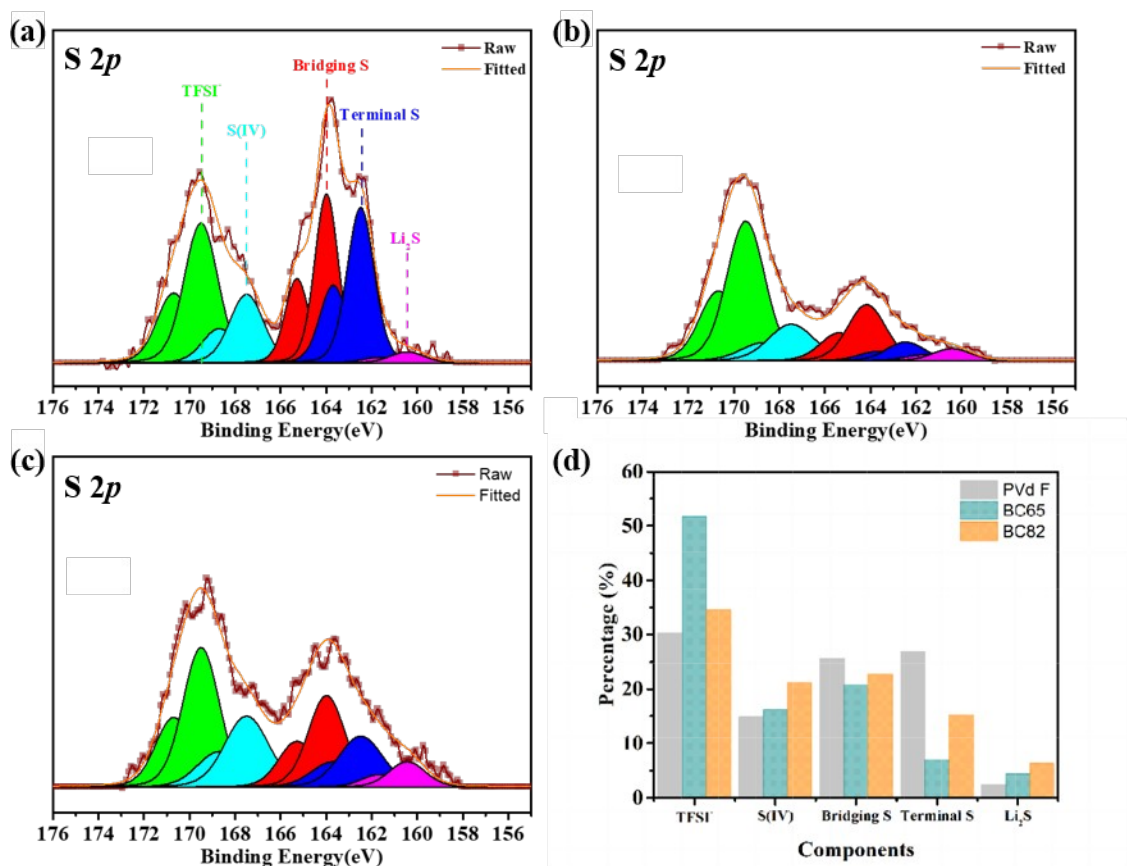


Fig. 5. Ex-situ XPS of S 2p spectra on the lithium anode surface after the third cycle: (a)-(c) correspond to the sulfur cathode with PVdF, BC65, and

BC82, respectively; the relative percentage of each component (d) is calculated based on the normalized peak area.

To confirm the influence of block copolymer on the polysulfide shuttle effect, the chemical composition on the surface of the lithium anode was studied. After the third cycle, the cells prepared with different binders were disassembled for XPS characterization. The results show that the surfaces of all the metallic lithium electrodes are covered by several sulfide species. S 2p peaks are split into two components (S 2p_{3/2} and S 2p_{1/2}) due to spin-orbit coupling, yielding pairs of peaks on the graph (Fig. 5). The main peak (S 2p_{3/2} at around 169.5 eV, in green) is assigned to the TFSI⁻ anion [46], which can be clearly observed from each electrode. The peak at a slightly lower binding energy (~167.5 eV, in cyan) is attributed to an S(IV) degradation species of the salt, which could be the Li₂SO₃ component [47]. The biggest differences for the spectrum of the cycled PVdF and block copolymer electrodes are the two components observed at low binding energy: ~164.1 eV (red) and ~162.1 eV (blue). These components are attributed to the bridging and terminal sulfur atoms of Li₂S_x polysulfides, respectively. The additional peak at lowest binding energies (~160.5 eV, in pink) represents Li₂S species, originating from the reduction of polysulfides into Li₂S at the surface of the metallic lithium anode. The relative peak intensity indicates the amount of polysulfides at the top surface of the metallic lithium anode (in 5 nm depth range), which could be used to analyze the diffusion and/or migration of these species from the sulfur composite cathode toward the lithium anode. Comparing the relative intensity ratios of components related to polysulfides decomposed on the studied anodes confirms the superior ability of block copolymer cathodes to confine polysulfides dissolution in the electrolyte. The effect is more apparent for samples prepared with BC65. A sample from the cell with BC82 contains a higher amount of polysulfides residue (although still significantly lower than in the cell with PVdF), especially Li₂S. This observation highlights the importance of the mechanical properties of the

binder derived from unswellable polystyrene groups. An optimal composition of ethylene oxide units and styrene units can provide a unique combination of physical and chemical properties, leading to enhanced stability in electrochemical cells.

4. Conclusion

In this study, high-performance Li-S batteries are developed using block copolymer as a multi-functional binder for the sulfur electrode. The function of ethylene oxide and styrene units involved in the polymer chain of binder for Li-S batteries is investigated, and the ratio of these components that enables better electrochemical performance is selected. The BC65 block copolymer combines the advantages of high mechanical strength, high ionic conductivity, and polysulfide trapping capability. The electrode prepared with the BC65 binder improves active materials utilization, facilitates reaction kinetics, maintains electrode integrity, and suppresses the shuttle effect. The initial specific discharge capacity of the cell using the BC65 binder can reach 1187 mAh g⁻¹ and stabilize at 708 mAh g⁻¹ after 50 cycles, which is superior to the performance of conventional PVdF-based electrodes. In situ UV-vis and operando XAS results show direct evidence that the ethylene oxide units can form strong chemical-trapping interactions with polysulfide intermediates. With the proper amount of the styrene unit to maintain mechanical strength, the designed binder could more effectively ameliorate the polysulfide dissolution and suppress the shuttle effect. In conclusion, the present study demonstrates a feasible and effective strategy to use multifunctional binder, which should be beneficial for the commercial application of high-energy Li-S batteries in the future.

Declaration of competing interest

The authors declare that they have no known competing financial interests or personal relationships that could have appeared to influence the work reported in this paper.

Acknowledgements

X.H., Z.M.L., G.L., and R.K. were supported by the Assistant Secretary for Energy Efficiency and Renewable Energy, Vehicle Technologies Office, under the Advanced Battery Materials Research (BMR) Program of the U.S. Department of Energy under Contract No. DE-AC02-05CH11231. X.T.L. acknowledge support by the U.S. Department of Energy under Contract No.106298-001. M.S. would like to acknowledge funding from Polish Ministry of Science and Higher Education No. 1670/MOB/V/2017/0. J.F. would like to acknowledge funding support of SUSTech. G.P.G and L.-W. W. used the resources of the National Energy Research Scientific Computing Center (NERSC) that is supported by the Office of Science of the U. S. Department of Energy.

References

- [1] M. Winter, B. Barnett, K. Xu, Chem. Rev. 118 (2018) 11433-11456.

- [2] Z. Zheng, H. Wu, H. Liu, Q. Zhang, X. He, S. Yu, V. Petrova, *ACS Nano* 14 (2020) 9545–9561.
- [3] X. Ji, K.T. Lee, L.F. Nazar, *Nat. Mater.* 8 (2009) 500–506.
- [4] P.G. Bruce, S.A. Freunberger, L.J. Hardwick, J.-M. Tarascon, *Nat. Mater.* 11 (2012) 19–29.
- [5] E. Environ, L. Ji, M. Rao, S. Aloni, L. Wang, J. Cairns, Y. Zhang, *Energy Environ. Sci.* 12 (2011) 5053–5059.
- [6] A. Manthiram, Y. Fu, S. Chung, C. Zu, Y. Su, *Chem. Rev.* 114 (2014) 11751–11787.
- [7] Z.W. Seh, Y. Sun, Q. Zhang, Y. Cui, *Chem. Soc. Rev.* 45 (2016) 5605–5634.
- [8] M. Wang, X. Xia, Y. Zhong, J. Wu, R. Xu, Z. Yao, D. Wang, W. Tang, X. Wang, J. Tu, *Chem. A Eur. J.* 25 (2018) 3710–3725.
- [9] H. Wang, Y. Yang, Y. Liang, J.T. Robinson, Y. Li, A. Jackson, *Nano Lett.* 11 (2011) 2644–2647.
- [10] L. Ji, M. Rao, H. Zheng, L. Zhang, Y. Li, W. Duan, J. Guo, E. J. Cairns, Y. Zhang, *J. Am. Chem. Soc.* 133 (2011) 18522–18525.
- [11] J. Guo, Y. Xu, C. Wang, *Nano Lett.* 11 (2011) 4288–4294.
- [12] Z. Zheng, P. Li, J. Huang, H. Liu, Y. Zao, Z. Hu, L. Zhang, H. Chen, M. Wang, D. Peng, Q. Zhang, *J. Energy Chem.* 41 (2020) 126–134.
- [13] F. Li, G. Zhou, S. Pei, L. Li, D.W. Wang, S. Wang, K. Huang, L.C. Yin, H.M. Cheng, *Adv. Mater.* 26 (2014) 625–631.
- [14] H. Yuan, J. Huang, H. Peng, M. Titirici, R. Xiang, R. Chen, Q. Liu, Q. Zhang, *Adv. Energy Mater.* 8 (2018) 1802107.
- [15] M.J. Lacey, F. Jeschull, K. Edstro, D. Brandell, *Chem. Commun.* (2013) 8531–8533.
- [16] F.-L. Zeng, N. Li, Y.-Q. Shen, X.-Y. Zhou, Z.-Q. Jin, N.-Y. Yuan, J.-Ni. Ding, A.-B. Wang, W.-K. Wang, Y.-Sh. Yang, *Energy Storage Mater.* 18 (2018) 190–198.
- [17] X. Li, Y. Cao, W. Qi, L. V. Saraf, J. Xiao, Z. Nie, J. Mietek, J.-G. Zhang, B. Schwenzera, J. Liu, *J. Mater. Chem.* 21 (2011) 16603–16610.
- [18] H. Zhang, X. Hu, Y. Zhang, S. Wang, F. Xin, X. Chen, D. Yu, *Energy Storage Mater.* 17 (2019) 293–299.
- [19] L. Hencz, H. Chen, H.Y. Ling, Y. Wang, C. Lai, H. Zhao, *Nano-Micro Lett.* (2019) 1–44.
- [20] B.A. Trofimov, L. V Morozova, M. V Markova, A.I. Mikhaleva, G.F.

- Myachina, I. V Tatarinova, T.A. Skotheim, *J. Appl. Polym. Sci.* 101 (2006) 4051-4055.
- [21] G. Li, M. Ling, Y. Ye, Z. Li, J. Guo, Y. Yao, J. Zhu, Z. Lin, Sh. ZHANG, *Adv. Energy Mater.* 5 (2015) 1500878.
- [22] J. Guo, Z. Yang, Y. Yu, L.A. Archer, *J. Am. Chem. Soc.* 135 (2013) 763-767.
- [23] W. Chen, T. Qian, J. Xiong, N. Xu, X. Liu, J. Liu, J. Zhou, X. Shen, T. Yang, Y. Chen, C. Yan, *Adv. Mater.* 29 (2017).
- [24] Z. Liu, X. He, C. Fang, L.E. Camacho-forero, Y. Zhao, Y. Fu, J. Feng, R. Kostecky, P.B. Balbuena, J. Zhang, J. Lei, G. Liu, *Adv. Funct. Mater.* 30 (2020) 2003605.
- [25] L.Y. Yang, D.X. Wei, M. Xu, Y.F. Yao, Q. Chen, *Angew. Chemie - Int. Ed.* 53 (2014) 3631-3635.
- [26] S.H. Chung, A. Manthiram, *Adv. Mater.* 26 (2014) 7352-7357.
- [27] W. Jia, Z. Cao, L. Wang, J. Fu, X. Chi, W. Gao, L.W. Wang, *Comput. Phys. Commun.* 184 (2013) 9-18.
- [28] W. Jia, J. Fu, Z. Cao, L. Wang, X. Chi, W. Gao, L.W. Wang, *J. Comput. Phys.* 251 (2013) 102-115.
- [29] J.P. Perdew, K. Burke, M. Ernzerhof, *Phys. Rev. Lett.* 77 (1996) 3865-3868.
- [30] J.P. Perdew, M. Ernzerhof, K. Burke, *J. Chem. Phys.* 105 (1996) 9982-9985.
- [31] A. Allouche, *J. Comput. Chem.* 32 (2012) 174-182.
- [32] R. Fayt, R. Jérôme, P. Teyssié, *J. Polym. Sci. Part B Polym. Phys.* 27 (1989) 775-793.
- [33] B. Brahimi, A. Ait-Kadi, A. Ajjji, R. Fayt, *J. Polym. Sci. Part B Polym. Phys.* 29 (1991) 945-961.
- [34] G. Xu, Q. bo Yan, A. Kushima, X. Zhang, J. Pan, J. Li, *Nano Energy* 31 (2017) 568-574.
- [35] K. Liu, A. Pei, H.R. Lee, B. Kong, N. Liu, D. Lin, Y. Liu, C. Liu, P. chun Hsu, Z. Bao, Y. Cui, *J. Am. Chem. Soc.* 139 (2017) 4815-4820.
- [36] W. Chen, T. Lei, T. Qian, W. Lv, W. He, C. Wu, X. Liu, J. Liu, B. Chen, C. Yan, J. Xiong, *Adv. Energy Mater.* 8 (2018) 1-8.
- [37] R. Carter, L. Oakes, N. Muralidharan, A.P. Cohn, A. Douglas, C.L. Pint, *ACS Appl. Mater. Interfaces* 9 (2017) 7185-7192.
- [38] J. Song, Z. Yu, M.L. Gordin, D. Wang, *Nano Lett.* 16 (2016) 864-870.

- [39] G. Zhang, Z. Zhang, H. Peng, J. Huang, Q. Zhang, 1700134 (2017) 1–32.
- [40] Q. Zou, Y. Lu, *J. Phys. Chem. Lett.* 7 (2016) 1518–1525.
- [41] M. Cuisinier, P.E. Cabelguen, S. Evers, G. He, M. Kolbeck, A. Garsuch, T. Bolin, M. Balasubramanian, L.F. Nazar, *J. Phys. Chem. Lett.* 4 (2013) 3227–3232.
- [42] K.H. Wujcik, T.A. Pascal, C.D. Pemmaraju, D. Devaux, W.C. Stolte, N.P. Balsara, D. Prendergast, *Adv. Energy Mater.* 5 (2015).
- [43] M.U.M. Patel, I. Arčon, G. Aquilanti, L. Stievano, G. Mali, R. Dominko, *ChemPhysChem* 15 (2014) 894–904.
- [44] L. Zhang, M. Ling, J. Feng, G. Liu, J. Guo, *Nano Energy* 40 (2017) 559–565.
- [45] P.P.R.M.L. Harks, C.B. Robledo, T.W. Verhallen, P.H.L. Notten, F.M. Mulder, *Adv. Energy Mater.* 7 (2017) 1–5.
- [46] R. Dedryvere, S. Leroy, H. Martinez, F. Blanchard, D. Lemordant, D. Gonbeau, *J. Phys. Chem. B* 110 (2006) 12986–12992.
- [47] D. Aurbach, E. Pollak, R. Elazari, G. Salitra, C.S. Kelley, J. Affinito, *J. Electrochem. Soc.* 156 (2009) 694–702.

Graphical abstract

The multiple functional binder for Li-S batteries is achieved via block polymer which integrate with different units in the polymer chain. The effects are revealed by operando ultraviolet-visible spectroscopy and S K-edge X-ray absorption spectroscopy.

